J Appl Electrochem (2007) 37:921–931
DOI 10.1007/s10800-007-9330-4

ORIGINAL PAPER

Prediction of shunt currents in a bipolar electrolyzer stack by difference calculus

Ravichandra S. Jupudi · Guillermo Zappi · Richard Bourgeois

Received: 21 December 2006 / Revised: 30 March 2007 / Accepted: 3 April 2007 / Published online: 25 May 2007

Abstract A model for predicting shunt/leakage currents in a bipolar electrolyzer stack with dual electrolyte inlets and significant amount of gases in the outlet ports and manifold is presented. Model includes electrolyte, manifold and membrane separator as resistance components in the electric circuit analog of the stack. Activation overvoltage associated with electrodes is taken as Tafel-like. Current balance and potential balance equations are applied to the stack and difference calculus is employed to reduce the problem to a set of linear difference equations with constant coefficients. The model is validated with published results and the effect of each resistance component and number of cells on leakage currents in the stack is presented.

Keywords Bipolar electrolyzer stack · Hydrogen production · Manifold current · Membrane separator · Shunt current

List of symbols

A_e	Area of the electrode, m^2
b	Constants in Eqs. 21 and 22
C_j	Independent constants to be determined from the boundary conditions
C_5^j	Constants in Eqs. 53–58
d	Depth of the inlet/outlet ports, m
D_j	Constants that are functions of r_j
E	Difference operator
E_j	Constants that are functions of r_j
E_C	Constant part of cell voltage, V
E_n	Cell voltage, V
E_o	Nernst potential, V
F	Faraday's constant, 96487 C mol^{-1}
F_j	Constants that are functions of r_j
g	Function that accounts for the increase in electrical resistivity due to the presence of gases
h_1	Width of the inlet/outlet port at the manifold end, m
h_2	Width of the inlet/outlet port at the electrode end, m
i_n^1	Cell current on the cathode side of the membrane, A
i_n^2	Cell current on the anode side of the membrane, A
i_o	Exchange current on the electrode, A
I	Direct current applied to the stack, A
I_S	Fraction of current lost in the form of parasitic currents
k_n	Leakage current in the cathodic inlet/outlet ports, A
K_n	Current in the manifold connected to the cathode sides of the electrolyzer cells, A
l_n	Leakage current in the anodic inlet/outlet ports, A
L_A	Gap between anode and the membrane , m
L_C	Gap between cathode and the membrane, m
L_M	Distance between two successive outlet ports, m
L_n	Current in the manifold connected to the anode sides of the electrolyzer cells, A
L_P	Thickness of the bipolar plate, m
L_S	Thickness of the membrane, m
N	Number of cells in the stack
N_M	McMullin number
r_j	Roots of the characteristic equation
R	Universal gas constant, J $mol^{-1}K^{-1}$
T	Stack operating temperature, K

R. S. Jupudi (✉)
Applied CFD Lab, GE Global Research, John F Welch Technology Centre Pvt Ltd, 122, EPIP, Phase 2, Whitefield Road, Hoodi Village, Bangalore, India
e-mail: ravichandra.js@ge.com

G. Zappi · R. Bourgeois
GE Global Research Center, Niskayuna, NY, USA

R_A Resistance in the inlet/outlet port on the anode side
R_C Resistance in the inlet/outlet port on the cathode side
R_{e1} Ohmic resistance in the cathodic electrolyte, Ω
R_{e2} Ohmic resistances in the anodic electrolyte, Ω
R_M Manifold resistance, Ω
R_S Resistance due to the membrane, Ω

Greek symbols

α_A Average volume fraction of O_2
α_C Average volume fraction of H_2
α_{eA} Average volume fraction of O_2 in the anode outlet port and anode manifold
α_{eC} Average volume fraction of H_2 in the cathode outlet port and cathode manifold
α_o Electrode transfer coefficient
η Electrode over voltage
θ Angle of the inlet/outlet port as shown in Fig. 3
ρ Electrical resistivity of pure electrolyte

Subscripts

i Pertaining to the inlet
e Pertaining to the outlet
n Pertaining to cell numbered n
A Pertaining to the anode electrode
C Pertaining to the cathode electrode

Superscripts

A Pertaining to the anode electrode
C Pertaining to the cathode electrode

1 Introduction

Hydrogen is evolving as a primary energy carrier of the future [1] as it can be used to store and transfer energy generated intermittently from renewable sources of energy. Among several methods of producing H_2, alkaline electrolysis is a well-understood technology and it promises to be a green energy alternative with no global warming effects. However, cost of H_2 produced via alkaline electrolysis is significantly higher in comparison to other hydrogen production technologies. This calls for innovation in alkaline electrolyzer cell and stack design.

Alkaline electrolyzer cells can be uni-polar or bipolar [1]. In a uni-polar cell, each electrode acts either as an anode or a cathode. In a bipolar cell, one side of the electrode acts as an anode and the other side acts as a cathode. Bipolar cells, hence lead to a very compact stack without any tabs and cell-to-cell inter-connections that are essential in a stack with unipolar cells. The compactness in design increases the energy density of the stack. However, an inherent limitation with a bipolar cell stack is leakage/shunt current [2]. Leakage current is the current that escapes from the main flow of cell current and passes through the electrolyte inlet, outlet ports and inlet, outlet manifolding. Leakage current reduces the efficiency of the stack. For optimum stack performance, stack design should be such that the leakage currents are minimal. The present work deals with the development of a model that will serve as a valuable tool in the design of such an electrolyzer stack.

Several papers dealt with the modeling of leakage currents in a bipolar electrolyzer stack [3–8]. Kuhn and Booth [3] reviewed the origins of bipolar leakage currents and computed leakage currents by modifying the zenor diode representation of the cell by Katz [4]. They incorporated the real i–V characteristics of the electrochemical cell by using a commercially available software package. Burnett and Danly [5] developed an analytical model for shunt currents by employing several simplifications. Without such simplifications, Dousek and Micka [6] used the Gauss elimination method to solve the $5N + 1$ equations representing the flow of currents in the electrolyzer stack. This model accounts for the presence of gases in the outlet ports and outlet manifolding, and assumes linear polarization at both the electrodes. Tafel polarization was incorporated by Rangarajan and Yegnanarayanan [7]. They analyzed leakage currents by solving the non-linear difference equations appropriate to Tafel regime by four different numerical methods. In order to keep the model simple, they neglected the effect of the presence of gases in the outlet ports and manifolding. In a subsequent paper, Rangarajan et al. [8] extended the model for current densities close to the electrode exchange current densities by including the effects of electrode over voltages by Butler–Volmer expressions.

In all the work discussed so far, attention was focused on simplifying the circuit analog of the electrolyzer stack by either neglecting the presence of gases or by assuming simple representation of the cell voltage. Not much attention was given to the relative importance of the individual resistance components of the cell. This is not justifiable as the membrane separator is an important contributor to the resistance of the cell. Further, the models discussed so far do not account for dual electrolyte inlets, which aid in reducing the leakage currents. By accounting for Tafel polarization at the electrodes and also for resistance due to the presence of gases, the present model appears more comprehensive than any of the existing models. Moreover, this model is computationally very inexpensive as it involves computation of the inverse of a 5×5 matrix only.

Model is validated by qualitative and quantitative comparison with published results. The effect of each of the resistance components and the number of cells on the percentage current lost in the form of parasitic currents is presented in Sect. 3. Section 3 is preceded by a detailed mathematical description of the model in Sect. 2.

2 Description of the model

It is an established practice to represent an electrolyzer stack by an equivalent circuit [3–8]. This inherently involves the assumption of uniform current distribution along the electrodes. Non-uniform current distribution can be accounted for by suitably coupling the electrolyzer circuit with a computational fluid dynamics (CFD) model of the kind reported by Mahmut Mat et al. [9, 10]. Figure 1 shows the resistances components and Fig. 2 shows the current components in the nth and $n+1$th cells of the circuit considered in the present work. In Fig. 1, resistances R_{e1} and R_{e2} are Ohmic resistances in the cathodic and anodic electrolytes respectively and R_S represents the resistance due to the membrane separating the anodic and cathodic channels. The increase in resistance due to the presence of gases is accounted via Maxwell Eq. [11]. The resistances are given by

$$R_{e1} = \frac{\rho L_C}{A_e}\left(\frac{1+\alpha_C/2}{1-\alpha_C}\right), \tag{1}$$

$$R_{e2} = \frac{\rho L_A}{A_e}\left(\frac{1+\alpha_A/2}{1-\alpha_A}\right) \tag{2}$$

and

$$R_S = \frac{\rho N_M L_S}{A_e}, \tag{3}$$

where N_M is McMullin number, defined as the ratio of the tortuosity to the porosity of the membrane [12]. The average volume fractions of gases in anodic and cathodic channels, outlet ports and outlet manifolds are obtained using a 3D CFD model developed along the lines of the 2D model of [9, 10]. The validated CFD model is in preparation for publication elsewhere.

In the current work, the inlet/outlet ports are considered to be trapezoidal in shape as shown in Fig. 3. A consideration that the surfaces of the electrolyte feed system are non-conducting, leads to the following expressions for resistances in the inlet/outlet ports

$$R^i_C = R^i_A = \frac{\rho}{2d\tan(\theta/2)}[\ln(h_2/h_1)], \tag{4}$$

$$R^e_C = R^i_C\left(\frac{1+\alpha_{eC}/2}{1-\alpha_{eC}}\right) \tag{5}$$

and

$$R^e_A = R^i_A\left(\frac{1+\alpha_{eA}/2}{1-\alpha_{eA}}\right), \tag{6}$$

The resistances in the inlet/outlet manifold are computed as follows

$$R^i_{MC} = R^i_{MA} = \frac{\rho L_M}{(\pi h_1^2/4)}, \tag{7}$$

$$R^e_{MC} = R^i_{MC}\left(\frac{1+\alpha_{eC}/2}{1-\alpha_{eC}}\right) \tag{8}$$

and

$$R^e_{MA} = R^i_{MA}\left(\frac{1+\alpha_{eA}/2}{1-\alpha_{eA}}\right), \tag{9}$$

where $L_M = L_C + L_A + L_S + L_P$ is the length between two successive outlet ports.

A constant direct current, which branches as it passes through the stack, is supplied to the circuit. The assumed direction of current flow is shown in Fig. 2. The main current, referred henceforth as cell current, is indicated as i^1_n and i^2_n on the cathode and anode sides of the membrane. The leakage currents, k_n and l_n in the cathodic and anodic inlet/outlet ports are considered perpendicular to the cell current. They are considered positive when they are flow-

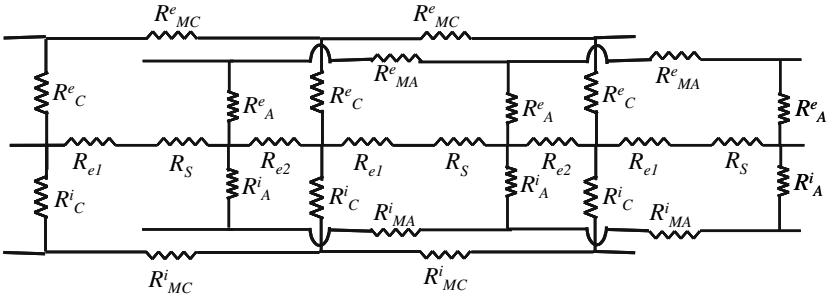

Fig. 1 Resistance components in a circuit analog of an N-cell assembly

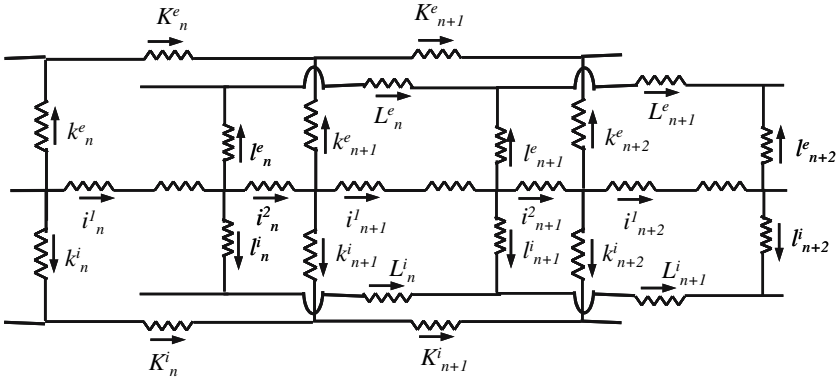

Fig. 2 Current components in a circuit analog of an *N*-cell assembly

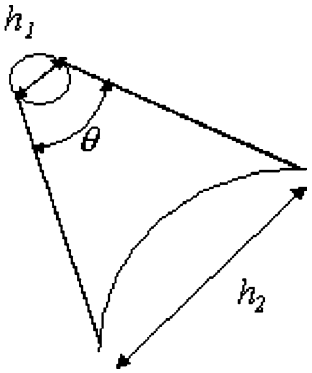

Fig. 3 Schematic of the electrolyte inlet/outlet triangle to the cell

ing towards the manifold and negative otherwise. The manifold currents, K_n and L_n are parallel to the cell current and are considered positive when they flow in the same direction as cell current and negative otherwise.

Ten simultaneous linear equations with ten variables: Four leakage currents (k^e_n ,k^i_n ,l^i_n ,l^e_n), four manifold currents (K^e_n ,K^i_n ,L^i_n ,L^e_n) and two battery currents result by applying Kirchoff's law to the *n*th cell of the network shown in Fig. 2. The first six equations are derived from the current balance equations at A, E, I, K B and G:

$$K^e_{n+1} - K^e_n - k^e_{n+1} = 0 \tag{10}$$

$$L^e_{n+1} - L^e_n - l^e_{n+1} = 0 \tag{11}$$

$$K^i_{n+1} - K^i_n - k^i_{n+1} = 0 \tag{12}$$

$$L^i_{n+1} - L^i_n - l^i_{n+1} = 0 \tag{13}$$

$$i^1_{n+1} - i^2_n + k^e_n + k^i_n = 0 \tag{14}$$

$$i^2_n - i^1_n + l^e_n + l^i_n = 0 \tag{15}$$

The other four equations are obtained by applying Kirchoff's second law to loops ABCD, EFGH, BIJC and FKLG:

$$R^e_C\left(k^e_{n+1} - k^e_n\right) - R^e_{MC}K^e_n + (R_{e1} + R_S)i^1_n + R_{e2}i^2_n + E_n = 0 \tag{16}$$

$$R^e_A\left(l^e_{n+1} - l^e_n\right) - R^e_{MA}L^e_n + (R_{e1} + R_S)i^1_{n+1} + R_{e2}i^2_n + E_n = 0 \tag{17}$$

$$R^i_C\left(k^i_{n+1} - k^i_n\right) - R^i_{MC}K^i_n + (R_{e1} + R_S)i^1_n + R_{e2}i^2_n + E_n = 0 \tag{18}$$

$$R^i_A\left(l^i_{n+1} - l^i_n\right) - R^i_{MA}L^i_n + (R_{e1} + R_S)i^1_{n+1} + R_{e2}i^2_n + E_n = 0 \tag{19}$$

In Eq. 16–19, E_n is cell voltage or voltage/potential sink for every cell. It is given by the sum of Nernst potential (E_o) and electrode over voltages (η_C , η_A) as follows

$$E_n = E_o + \eta_C + \eta_A \tag{20}$$

A general equation for the computation of electrode over-voltage is the Butler–Volmer Equation [8]. However, Tafel equation [7] is a very good approximation for the current potential relationship when the applied current is significantly higher than the electrode exchange current. Hence, the electrode over-voltages are taken as

$$\eta_C = b_C \ln\left(\frac{i^1_n}{i^C_o}\right) \tag{21}$$

and

$$\eta_A = b_A \ln\left(\frac{i^2_n}{i^A_o}\right), \tag{22}$$

where

$$b_C = \frac{RT}{\alpha^C_o F}; \quad b_a = \frac{RT}{\alpha^A_o F}. \tag{23}$$

Following [7], the over-voltages are approximated as

$$\eta_C = b_C \ln\left(\frac{i_n^1}{i_o^C}\right) = b_C \ln\left(\frac{I}{i_o^C}\right) - b_C\left(\frac{k_n^e + k_n^i}{I}\right) \tag{24}$$

$$\eta_A = b_A \ln\left(\frac{i_n^2}{i_o^A}\right) = b_A \ln\left(\frac{I}{i_o^A}\right) - b_A\left(\frac{l_n^e + l_n^i}{I}\right). \tag{25}$$

For the sake of convenience, the expression for cell voltage is written as

$$E_n = E_C - b_C\left(\frac{k_n^e + k_n^i}{I}\right) - b_A\left(\frac{l_n^e + l_n^i}{I}\right) \tag{26}$$

where

$$E_C = E_o + b_C \ln\left(\frac{I}{i_o^C}\right) + b_A \ln\left(\frac{I}{i_o^A}\right) \tag{27}$$

is the constant part of the cell voltage term.

Following [2], Eqs. 10–19 are rewritten in the form of linear difference equations as follows

$$(E-1)K^e - Ek^e = 0 \tag{28}$$

$$(E-1)L^e - El^e = 0 \tag{29}$$

$$(E-1)K^i - Ek^i = 0 \tag{30}$$

$$(E-1)L^i - El^i = 0 \tag{31}$$

$$Ei^1 - i^2 + E\left(k^e + k^i\right) = 0 \tag{32}$$

$$i^2 - i^1 + l^e + l^i = 0 \tag{33}$$

$$R_C^e(E-1)k^e - R_{MC}^e K^e + (R_{e1} + R_S)i^1 + R_{e2}i^2 + E_C - b_C\left(\frac{k^e + k^i}{I}\right) - b_A\left(\frac{l^e + l^i}{I}\right) = 0 \tag{34}$$

$$R_A^e(E-1)l^e - R_{MA}^e L^e + (R_{e1} + R_S)Ei^1 + R_{e2}i^2 + E_C - b_C\left(\frac{k^e + k^i}{I}\right) - b_A\left(\frac{l^e + l^i}{I}\right) = 0 \tag{35}$$

$$R_C^i(E-1)k^i - R_{MC}^i K^i + (R_{e1} + R_S)i^1 + R_{e2}i^2 + E_C - b_C\left(\frac{k^e + k^i}{I}\right) - b_A\left(\frac{l^e + l^i}{I}\right) = 0 \tag{36}$$

$$R_A^i(E-1)l^i - R_{MA}^i L^i + (R_{e1} + R_S)Ei^1 + R_{e2}i^2 + E_C - b_C\left(\frac{k^e + k^i}{I}\right) - b_A\left(\frac{l^e + l^i}{I}\right) = 0 \tag{37}$$

where

$$K^e = K_n^e; K^i = K_n^i; k^e = k_n^e; k^i = k_n^i, \tag{38}$$

$$L^e = L_n^e; L^i = L_n^i; l^e = l_n^e; l^i = l_n^i, \tag{39}$$

and

$$i^1 = i_n^1; i^2 = i_n^2. \tag{40}$$

E is the difference operator defined as [2]

$$Ef(x) = f(x+1) \tag{41}$$

and

$$E^n f(x) = f(x+n). \tag{42}$$

Appropriate mathematical treatment of Eqs. 34–37 leads to

$$k^i = k^e g(\alpha_{eC}) \tag{43}$$

and

$$l^i = l^e g(\alpha_{eA}), \tag{44}$$

where function g, that accounts for the increase in electrical resistivity due to the presence of gases, is defined as [11]

$$g(\alpha) = \frac{(1 + \alpha/2)}{(1-\alpha)} \tag{45}$$

Eliminating K^e, L^e, k^i, l^i, $i^1$and i^2 from Eqs. 34 to 35, we get

$$\left[R_C^e(E-1)^2 - \left\{R_{MC}^e + \left(1+g(\alpha_{eC})\right)\left(R_{e1}+R_S+R_{e2}+\frac{b_C}{I}\right)\right\}E + \frac{b_C}{I}\left(1+g(\alpha_{eC})\right)\right]k^e - \left(1+g(\alpha_{eC})\right)\left[\left(R_{e2}-\frac{b_A}{I}\right)E + R_{e1} + R_S + \frac{b_A}{I}\right]l^e = 0 \tag{46}$$

$$\left[R_A^e(E-1)^2 - \left\{R_{MA}^e + \left(1+g(\alpha_{eA})\right)\left(R_{e1}+R_S+R_{e2}+\frac{b_A}{I}\right)\right\}E + \frac{b_A}{I}\left(1+g(\alpha_{eA})\right)\right]l^e - \left(1+g(\alpha_{eA})\right)\left[\left(R_{e1}+R_S\right)E^2 + \left(R_{e2}-\frac{b_C}{I}\right)E + \frac{b_C}{I}\right]k^e = 0 \tag{47}$$

$$\begin{aligned}&\left[R_C^e(E-1)^2-\left\{R_{MC}^e+(1+g(\alpha_{eC}))\left(R_{e1}+R_S+R_{e2}+\frac{b_C}{I}\right)\right\}E+\frac{b_C}{I}(1+g(\alpha_{eC}))\right]\\&\times\left[R_A^e(E-1)^2-\left\{R_{MA}^e+(1+g(\alpha_{eA}))\left(R_{e1}+R_S+R_{e2}+\frac{b_A}{I}\right)\right\}E+\frac{b_A}{I}(1+g(\alpha_{eA}))\right]k^e\\&-(1+g(\alpha_{eC}))(1+g(\alpha_{eA}))\\&\times\left[\left(R_{e2}-\frac{b_A}{I}\right)E+R_{e1}+R_S+\frac{b_A}{I}\right]\left[(R_{e1}+R_S)E^2+\left(R_{e2}-\frac{b_C}{I}\right)E+\frac{b_C}{I}\right]k^e=0\end{aligned}\tag{48}$$

Further eliminating l^e from Eq. 46, using Eq. 47, we get

Equation 48 is a fourth order linear homogeneous difference equation with constant coefficients. Considering that the characteristic equation corresponding to this equation does not have multiple roots, the general solution for k^e can be written as

$$k^e=\sum_{j=1}^{4}C_jr_j^n\tag{49}$$

where C_j are independent arbitrary constants to be determined from the boundary conditions and r_j are the roots of the characteristic equation. Further, the general solutions for l^e, k^i, and l^i can be written as

$$l^e=\sum_{j=1}^{4}C_jD_jr_j^n,\tag{50}$$

$$k^i=\sum_{j=1}^{4}C_jE_jr_j^n\tag{51}$$

and

$$l^i=\sum_{j=1}^{4}C_jF_jr_j^n,\tag{52}$$

where D_j, E_j and F_j are constants that are functions of r_j. They can be determined once the general solutions are obtained.

Using the general solution for k^e in Eq.28, we get the general solution for K^e as

$$K^e=C_5^1+\sum_{j=1}^{4}\frac{C_jr_j^{n+1}}{r_j-1}.\tag{53}$$

Similarly, the general solutions for L^e, K^i, L^i, $i^1$and i^2 are found to be

$$L^e=C_5^2+\sum_{j=1}^{4}\frac{C_jD_jr_j^{n+1}}{r_j-1},\tag{54}$$

$$K^i=C_5^3+\sum_{j=1}^{4}\frac{C_jE_jr_j^{n+1}}{r_j-1},\tag{55}$$

$$L^i=C_5^4+\sum_{j=1}^{4}\frac{C_jF_jr_j^{n+1}}{r_j-1},\tag{56}$$

$$i^1=C_5-\sum_{j=1}^{4}C_j\left(D_j+E_jr_j+F_j+r_j\right)\frac{r_j^n}{r_j-1}\tag{57}$$

and

$$i^2=C_5-\sum_{j=1}^{4}C_j\left(D_j+E_j+F_j+1\right)\frac{r_j^{n+1}}{r_j-1}.\tag{58}$$

In Eqs. 53–58, C_5^1 , C_5^2 , $C_5^3$and C_5^4 are constants. They can be obtained by substituting the general solutions of the current components [Eqs. 49–58] in Eqs. 34 and 35 and equating the resultant coefficients of terms with identical exponents. This results in the following expressions for C_5^1 to C_5^4, D_j, E_j and F_j,

$$C_5^1=\frac{R_{e1}+R_S+R_{e2}}{R_{MA}^e}+\frac{E_C}{R_{MA}^e},\tag{59}$$

$$C_5^2=\frac{R_{e1}+R_S+R_{e2}}{R_{MC}^e}+\frac{E_C}{R_{MC}^e},\tag{60}$$

$$C_5^3=\frac{R_{e1}+R_S+R_{e2}}{R_{MA}^i}+\frac{E_C}{R_{MA}^i},\tag{61}$$

$$C_5^4=\frac{R_{e1}+R_S+R_{e2}}{R_{MC}^i}+\frac{E_C}{R_{MC}^i},\tag{62}$$

$$E_j=g(\alpha_{eC}),\tag{63}$$

$$D_j=\frac{F_j}{g(\alpha_{eA})}\tag{64}$$

and

$$D_j+F_j=\frac{R_A^e\left(r_j-1\right)^2-\left[(R_{e1}+R_S+R_{e2})(1+g(\alpha_{eC}))+R_{MA}^e\right]r_j}{R_{e1}+R_S+R_{e2}r_j}. \tag{65}$$

This reduces the unknowns to the roots of the characteristic equation corresponding to Eq. 48 and coefficients C_j. The roots r_j, can be obtained by substituting Eq. 49 in Eq. 48. Equation 48 thus transforms to

$$Ar^4 - Br^3 + Cr^2 - Hr + I = 0 \tag{66}$$

where

$$A = R_A^e R_C^e, \tag{67}$$

$$\begin{aligned} B =& R_A^e\left[2R_C^e+R_{MC}^e+(1+g(\alpha_{eC}))\left(R_{e1}+R_S+R_{e2}+\frac{b_C}{I}\right)\right] \\ &+R_C^e\left[2R_A^e+R_{MA}^e+(1+g(\alpha_{eA}))\left(R_{e1}+R_S+R_{e2}+\frac{b_A}{I}\right)\right] \\ &-(1+g(\alpha_{eC}))(1+g(\alpha_{eA}))(R_{e1}+R_S)\left(R_{e2}-\frac{b_A}{I}\right), \end{aligned} \tag{68}$$

$$\begin{aligned} C =& 2R_A^e R_C^e \\ &+\left[2R_A^e+R_{MA}^e+(1+g(\alpha_{eA}))\left(R_{e1}+R_S+R_{e2}+\frac{b_A}{I}\right)\right] \\ &\times\left[2R_C^e+R_{MC}^e+(1+g(\alpha_{eC}))\left(R_{e1}+R_S+R_{e2}+\frac{b_C}{I}\right)\right] \\ &-(1+g(\alpha_{eC}))(1+g(\alpha_{eA}))\left[(R_{e1}+R_S)\left(R_{e1}+R_S+\frac{b_A}{I}\right)\right. \\ &\left.-\left(R_{e2}-\frac{b_C}{I}\right)\left(R_{e2}-\frac{b_A}{I}\right)\right], \end{aligned} \tag{69}$$

$$\begin{aligned} H =& R_A^e\left[2R_C^e+R_{MC}^e+(1+g(\alpha_{eC}))\left(R_{e1}+R_S+R_{e2}+\frac{b_C}{I}\right)\right] \\ &+R_C^e\left[2R_A^e+R_{MA}^e+(1+g(\alpha_{eA}))\left(R_{e1}+R_S+R_{e2}+\frac{b_A}{I}\right)\right] \\ &-(1+g(\alpha_{eC}))(1+g(\alpha_{eA}))\left[\left(R_{e1}+R_S+\frac{b_A}{I}\right)\left(R_{e2}-\frac{b_C}{I}\right)\right. \\ &\left.+\frac{b_C}{I}\left(R_{e2}-\frac{b_A}{I}\right)\right] \end{aligned} \tag{70}$$

and

$$I = R_A^e R_C^e - (1+g(\alpha_{eC}))(1+g(\alpha_{eA}))\frac{b_C}{I}\left(R_{e1}+R_S+\frac{b_A}{I}\right) \tag{71}$$

Equation 66 is a fourth order polynomial, which may be solved for r_j without much difficulty.

Finally, C_j (C_1 to C_5) are obtained using the following five boundary conditions:

$$K_0^e = 0 \Rightarrow \sum_{j=1}^{4}\frac{C_j r_j}{r_j-1}+\frac{R_{e1}+R_S+R_{e2}}{R_{MA}^e}+\frac{E_C}{R_{MA}^e}=0 \tag{72}$$

$$K_N^e = 0 \Rightarrow \sum_{j=1}^{4}\frac{C_j r_j^{N+1}}{r_j-1}+\frac{R_{e1}+R_S+R_{e2}}{R_{MA}^e}+\frac{E_C}{R_{MA}^e}=0 \tag{73}$$

$$L_0^e = 0 \Rightarrow \sum_{j=1}^{4}\frac{C_j D_j r_j}{r_j-1}+\frac{R_{e1}+R_S+R_{e2}}{R_{MC}^e}+\frac{E_C}{R_{MC}^e}=0 \tag{74}$$

$$L_N^e = 0 \Rightarrow \sum_{j=1}^{4}\frac{C_j D_j r_j^{N+1}}{r_j-1}+\frac{R_{e1}+R_S+R_{e2}}{R_{MC}^e}+\frac{E_C}{R_{MC}^e}=0 \tag{75}$$

$$i_1^1+k_1^i+k_1^e = I \Rightarrow -\sum_{j=1}^{4}C_j\left(D_j+E_j+F_j+1\right)\frac{r_j}{r_j-1}+C_5 = I \tag{76}$$

In Eqs. 72–76, all the resistance components and E_C, r_j, D_j, E_j and F_j are known. Hence coefficients, C_j can be easily obtained by inverting the 5 × 5 matrix represented by Eqs. 72–76. Once the coefficients C_j are obtained, Eqs. 49–58 form a closed set of final expressions for various current components of the bipolar electrolyzer stack.

3 Results and discussion

Leakage/shunt currents are a function of all the resistances and the number of cells. This section presents a summary of a systematic study on the effect of varying each of the resistances as well as the number of cells on leakage currents. Numerical values of a baseline case considered in this study are listed in Table 1.

Figure 4 shows the variation of leakage current and manifold current in the cathode side outlet ports and outlet manifold respectively and Fig. 5 shows the variation of cell current on the cathode and anode sides of the membrane pertaining to the resistances listed in Table 1. Leakage current is maximum in magnitude in the outermost cells and it changes sign in the central portion of the stack. Manifold current increases in the direction of cell current up to the central part of the stack and decreases thereafter. Hence the cell current, as shown in Fig. 5, is maximum in the outermost cells and minimum in the central portion of the stack. Further, due to the presence of the membrane,

Table 1 Parameters corresponding to baseline case

Symbol	Value	Units
$R_{e1} = R_{e2}$	0.0002	Ω
R_S	0.00005	Ω
$R^i_C = R^i_A$	2	Ω
$R^i_{MC} = R^i_{MA}$	0.025	Ω
α_C	0.1	
α_A	0.15	
α_{eC}	0.2	
α_{eA}	0.2	
i^C_o	0.1	A
i^A_o	0.1	A
I	1000	A
N	20	
E_o	1.18	V

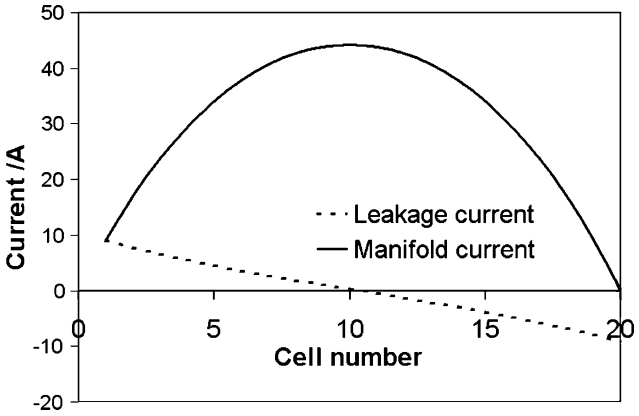

Fig. 4 Leakage and manifold currents across the cell stack

variation of cell current is not same on the cathode and anode sides of the membrane. On the cathode sides, cell current is symmetric about the central cell whereas it is asymmetric on the anode sides of the membrane. The

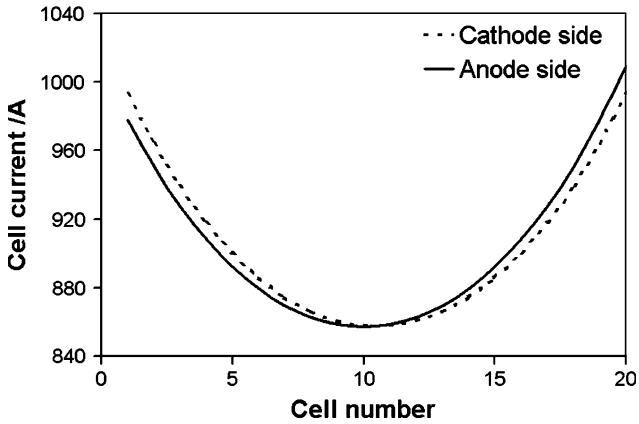

Fig. 5 Cell current on cathode and anode sides of the cell stack

Table 2 Parameters of case from [7] considered for validation

Symbol	Value	Units
$R_{e1} = R_{e2}$	4.9	Ω
	800	Ω
$R^i_{MC} = R^i_{MA}$	4.9	Ω
i^C_o/A_e	84	A/m^2
i^A_o/A_e	84	A/m^2
I	0.1	A
E_o	2.4	V

asymmetry can be expected to increase with increase in the membrane resistance. These intuitively appealing results are in qualitative accordance with published literature [7, 8]. However, a quantitative agreement with relevant experimental data establishes full validation of the model. In the absence of experimental data, the present model is verified by simulating the results reported by [7]. The model of [7] is less complicated as it does not account for the presence of gases and is for a stack design without dual inlets. Further, only a single aggregate resistance represents each cell in the model of [7]. However, results of [7] are significant in verifying the current model, as the authors of [7] establish the validity of their results using four different numerical methods. Table 2 lists the numerical details of test cases of [7] considered in the present study for the sake of comparison. Figure 6 shows the manifold currents computed using the current model with resistance and load current inputs from [7]. Computed results are found to be within 2% error with the results of [7]. This lends confidence in the validity of the current model.

Currents leak into the inlet/outlet ports from both cathode and anode compartments. Hence, a parameter of significance is the total percentage of current lost (I_S)in the form of parasitic currents. It is computed as

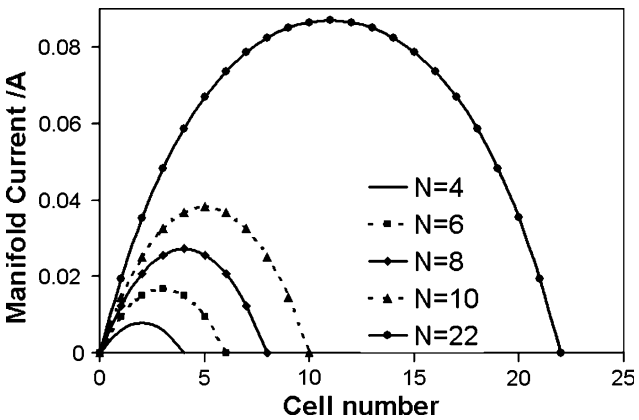

Fig. 6 Comparison of predicted manifold currents with the results of [7]

$$I_S\% = \left[\frac{NI - \sum_{j=1}^{N} i_j^1}{NI} + \frac{NI - \sum_{j=1}^{N} i_j^2}{NI}\right] \times 100 \qquad (77)$$

In all the following sections, leakage currents are assessed by the changes in this parameter.

3.1 Effect of internal resistances of the cell

The baseline values for the internal resistances R_{e1} , R_S and R_{e2} are 0.2, 0.2 and 0.05 mΩ respectively. In order to study the effect of varying these resistances, each of them is varied in steps of 0.1 mΩ (50% of baseline value) while holding the other two constant. Increasing one resistance component while holding the other two constant increases the total internal resistance by 0.1 mΩ. The number of cells is held constant at 20. Figure 7 shows results obtained by such an exercise. The total percentage loss in the form of parasitic currents increases with increase in the total internal resistance of the cell. This increase in I_S, is however almost independent of whether the increase in R is because of increase in R_{e1} or R_S or R_{e2}. The obvious reason for this independence of I_S on the internal resistance components of the cell is the three orders of magnitude difference between the inlet/outlet port resistances and the internal resistances.

3.2 Effect of resistances in the inlet/outlet ports

Figures 8 and 9 show the effect of increasing the resistance of the inlet/outlet ports on the percentage of current lost in the form of parasitic currents. With increase in the inlet/outlet port resistance, I_S decreases in general and at high values of inlet/outlet port resistance, I_S reduces to zero asymptotically.

Figure 8 shows that at a particular R_A, I_S increases with increase in N. The obvious reason for this increase in I_S with increase in N is the increase in the number of paths for the flow of shunt currents. However, Fig. 9 shows that at a particular R_A, I_S decreases with increase in I. This result is a consequence of the Ohm's law. Since the internal resistance of the cell is much less than the shunt resistances, the percentage of current passing through the bypass paths decreases with increase in I.

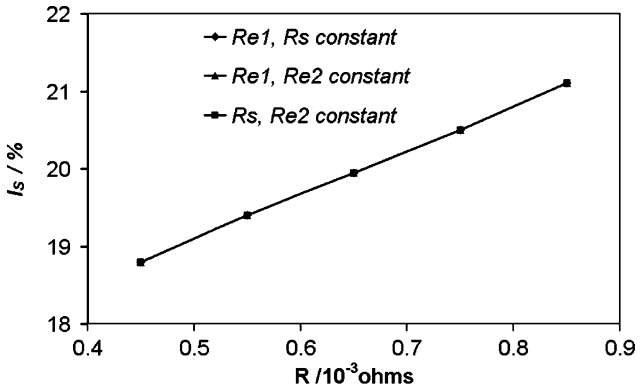

Fig. 7 Effect of various components of cell internal resistance on I_S

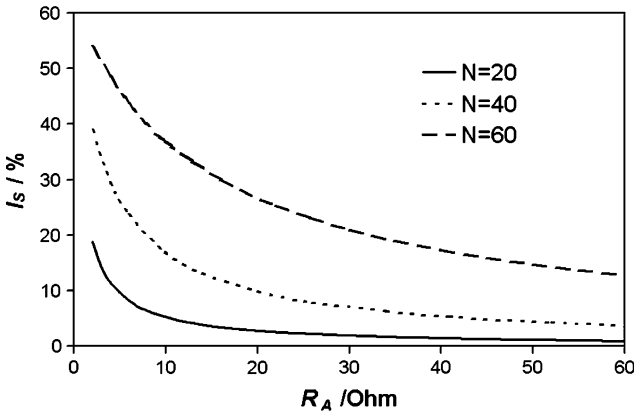

Fig. 8 Effect of inlet/outlet port resistance on I_S at several N

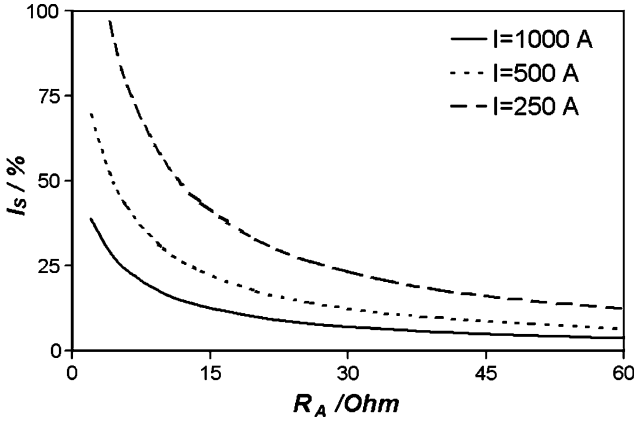

Fig. 9 Effect of inlet/outlet port resistance at several I

3.3 Effect of manifold resistances

Figures 10 and 11 show the effect of increasing the manifold resistances (R_{MA}, R_{CA}) on the percentage of current lost in the form of parasitic currents. Figure 10 shows that I_S decreases with increase in R_{MA}. An important point to note is that I_S tends to become independent of N as R_{MA} approaches R_A. Therefore in order to facilitate the incorporation of more cells in a stack, the manifold should be designed such that $R_{MA} \approx R_A$. No such independence of I_S on N can be observed in Fig. 11 even at $R_{MA} = R_A$. I_S decreases monotonically with R_{MA} at all N, following Ohm's law.

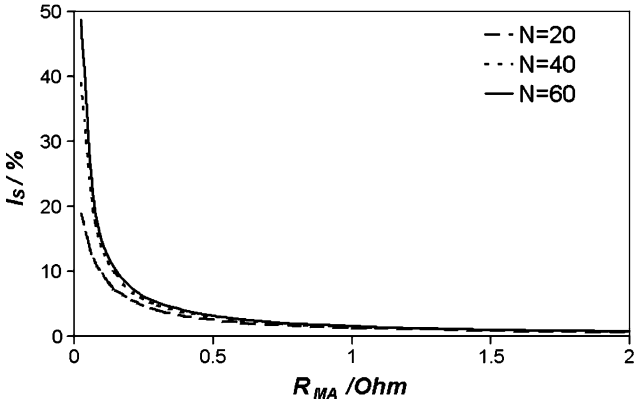

Fig. 10 Effect of manifold resistance on I_S at several N

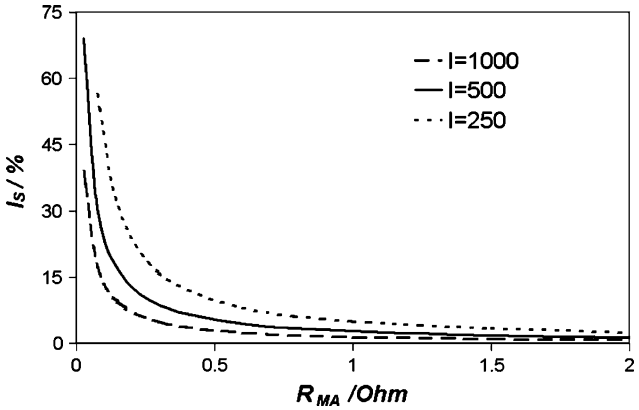

Fig. 11 Effect of manifold resistance on I_S at several I

3.4 Effect of volume fraction of the gases

The presence of gases increases the resistance in the outlet ports and outlet manifold. In the present work, this increase in resistance due to the presence of gases is accounted for via the Maxwell equation [11]. Figures 12 and 13 show the effect of the volume fraction of gases on I_S. I_S decreases linearly with the average volume fraction of the gases at all N and I. This is as expected as the Maxwell equation indicates a nearly linear increase (shown in Fig. 14) in the outlet port resistance with increase in the average volume fraction of the gases. However, a point to note is that the magnitude of the slope of the linear plots in Fig. 12 and 13 is greater at higher N and lower I.

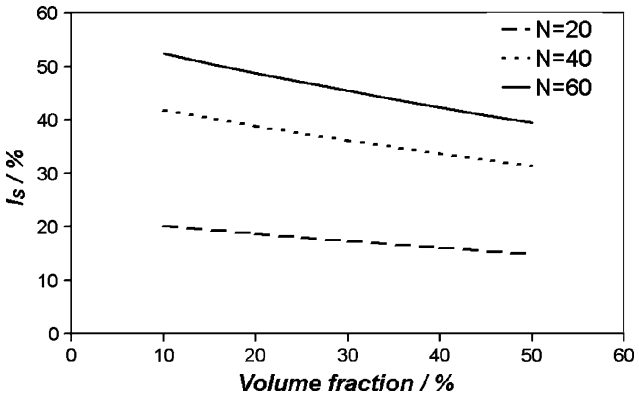

Fig. 12 Effect of gas volume fraction on I_S at several N

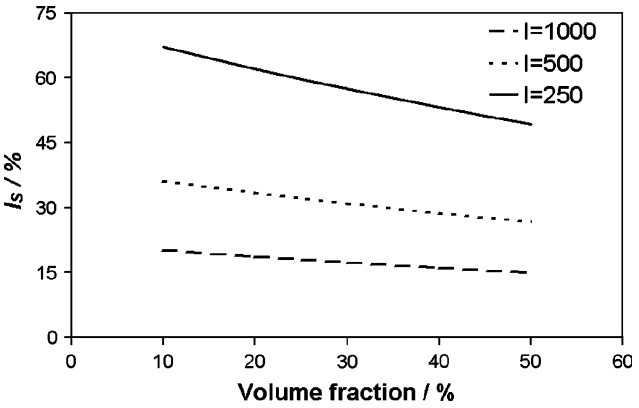

Fig. 13 Effect of gas volume fraction on I_S at several I

3.5 Effect of number of cells

The effect of varying various resistance components individually at different N is presented in the previous sections. In this section, the effect of the number of cells is studied by varying all the shunt resistances by a fraction, while holding the internal resistances of the cells constant. For the sake of clarity, the shunt resistances corresponding to the base line case are represented by R_b. In Fig. 15, R_b indicates $R^i_A = R^i_C = 2\ \Omega$ and $R^i_{MA} = R^i_{MC} = 25\ m\ \Omega$ and R_{kb} indicates $R^i_A = R^i_C = 2k\Omega$ and $R^i_{MA} = R^i_{MC} = 25k\text{m}\ \Omega$. Figure 15 shows that I_S increases with N irrespective of the magnitude of the shunt resistances. However, an important point to note is that as the shunt resistances increase, the

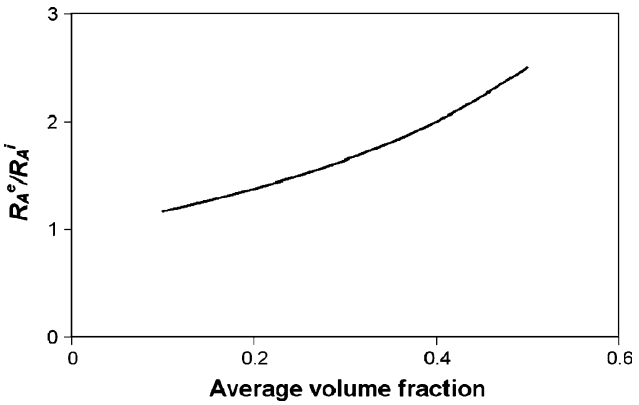

Fig. 14 Effect of gas volume fraction on outlet port resistance

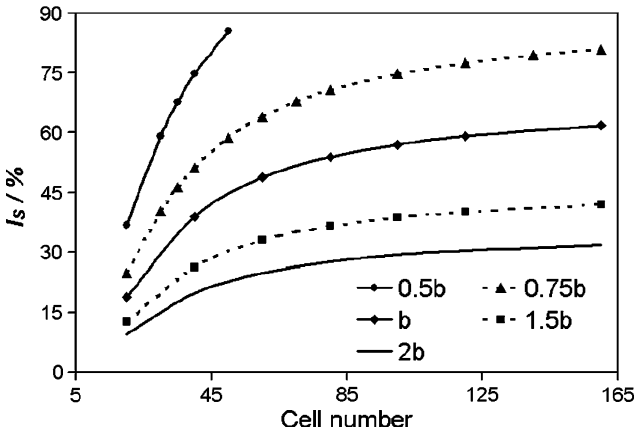

Fig. 15 Effect of N on I_S

effect of the number of cells decreases. In the cases of $R_{1.5b}$ and R_{2b}, beyond $N = 60$, I_S increases only by about 1% for every 10 additional cells. Therefore, a point of practical importance is that a large number of cells can be incorporated without significant increase in I_S, by ensuring that the shunt resistances are sufficiently high.

4 Conclusions

1. The method of difference calculus is found to be very efficient for computing the shunt currents in an alkaline electrolyzer stack. This involves computing the inverse of a 5×5 matrix only for a stack of any number of cells. On the other hand, the matrix inverse method involves computing the inverse of a $N \times N$ matrix.
2. The model is found to replicate published data qualitatively as well as quantitatively.
3. Percentage of current lost in the form of shunt current increases with increase in the total internal resistance of the cell.
4. Overall loss due to shunt currents decreases non-linearly with increase in inlet port resistance up to a certain limit. Beyond this limit, overall loss due to shunt currents reduces to zero asymptotically. Knowing this limit would be quite useful in the design of inlet/outlet ports.
5. When all the resistances are kept constant, percentage loss due shunt currents increases with increase in the number of cells. Percentage loss however decreases with increase in load current.
6. Loss due to shunt currents decreases with increase in the manifold resistance. It becomes independent of the number of cells as the manifold resistance approaches the inlet port resistance.
7. Presence of gases in the outlet port and outlet manifold is found to affect the loss due to shunt currents. Loss due to shunt currents is found to vary linearly with the average volume fraction of the gases in the neck and manifold.
8. The effect of the number of cells on overall loss due to shunt currents becomes insignificant at high shunt resistances. However, at low shunt resistances, loss due to shunt currents increases almost linearly with the number of cells.

Acknowledgements The second and third authors of this paper gratefully acknowledge financial support provided by the U.S. Department of Energy under Award Number DE-FC-14223.*Disclaimer*: ''This report was prepared as an account of work sponsored by an agency of the United States Government. Neither the United States Government nor any agency thereof, nor any of their employees, makes any warranty, express or implied, or assumes any legal liability or responsibility for the accuracy, completeness, or usefulness of any information, apparatus, product, or process disclosed, or represents that its use would not infringe privately owned rights. Reference herein to any specific commercial product, process, or service by trade name, trademark, manufacturer, or otherwise does not necessarily constitute or imply its endorsement, recommendation, or favoring by the United States Government or any agency thereof. The views and opinions of authors expressed herein do not necessarily state or reflect those of the United States Government or any agency thereof.''

References

1. Ulleberg O (2003) Int J Hydrogen Energy 28:21
2. Yang MZ, Wu H, Robert Selman J (1989) J Appl Electrochem 19:247
3. Kuhn AT, Booth JS (1980) J Appl Electrochem 10:233
4. Katz M (1978) J Electrochem Soc 125(4):515
5. Burnett JC, Danly DE (1979) AIChE Symposium Series 75(185):8
6. Dousek FP, Micka K (1993) J Appl Electrochem 23:241
7. Rangarajan SK, Yegnanarayanan V (1997) Electochimica Acta 42:153
8. Rangarajan SK, Yegnanarayanan V, Muthukumar M (1998) Electochimica Acta 44:491
9. Mat MD, Aldas K, Ilegbusi OJ (2004) Int J Hydrogen Energy 29(10):1015
10. Mat MD, Aldas K (2005) Int J Hydrogen Energy 30(4):411
11. Maxwell JC (1881) A treatise on electricity and magnetism, 2nd edn. Clarendon Press, Oxford
12. Van Zee J, White RE, Watson AT (1986) J Electrochem Soc:Electrochem Sci Technol 133(3):501